Dielectric and optical properties of superlattices of epitaxially connected nanocrystals

Christophe Delerue, P. Tim Prins, Daniel Vanmaekelbergh, Zeger Hens

▶ **To cite this version:**

Christophe Delerue, P. Tim Prins, Daniel Vanmaekelbergh, Zeger Hens. Dielectric and optical properties of superlattices of epitaxially connected nanocrystals. Physical Review B, 2023, 107 (24), pp.245413. 10.1103/PhysRevB.107.245413 . hal-04126088

HAL Id: hal-04126088
https://hal.science/hal-04126088

Submitted on 15 Jun 2023

HAL is a multi-disciplinary open access archive for the deposit and dissemination of scientific research documents, whether they are published or not. The documents may come from teaching and research institutions in France or abroad, or from public or private research centers.

L'archive ouverte pluridisciplinaire **HAL**, est destinée au dépôt et à la diffusion de documents scientifiques de niveau recherche, publiés ou non, émanant des établissements d'enseignement et de recherche français ou étrangers, des laboratoires publics ou privés.

Dielectric and optical properties of superlattices of epitaxially connected nanocrystals

Christophe Delerue *
University of Lille, CNRS, Centrale Lille, University Polytechnique Hauts-de-France, Junia, UMR 8520 - IEMN, F-59000 Lille, France

P. Tim Prins and Daniel Vanmaekelbergh
Debye Institute for Nanomaterials Science, University of Utrecht, Princetonplein 1, 3584 CC Utrecht, The Netherlands

Zeger Hens
Physics and Chemistry of Nanostructures (PCN), Ghent University, 9000 Gent, Belgium

(Received 28 October 2022; revised 17 April 2023; accepted 5 June 2023; published 12 June 2023)

Colloidal semiconductor nanocrystals (NCs) are believed to strongly absorb resonant light; this property is key to ongoing applications of NCs as phosphor in light-emitting diodes (LEDs) for lighting, in displays, and photodetectors. However, it has been realized that NCs in a low dielectric medium suffer from a weak permeation of the electromagnetic field in the solid due to formation of depolarization fields, strongly reducing light absorption, as quantified by the local-field factor. For low-dimensional semiconductors, such as one-dimensional (1D) rods and two-dimensional (2D) superlattices, this depolarization field depends critically on the electromagnetic field direction versus the long direction of the material. Here we present atomistic calculations of the screening of the electromagnetic field for individual NCs and technologically important architectures, i.e., 1D and 2D superlattices of epitaxially connected NCs. We also investigate the combined effects of epitaxial connections and excitonic interactions in the particular case of dimers of NCs. Even if it can be improved by a matrix of high dielectric constant, the local-field factor of individual NCs is very low but can increase more than an order of magnitude in NC chains or NC superlattices for an in-line or in-plane electromagnetic field. The calculations of the optical absorptance agree with recent experimental results obtained on superlattices of PbSe and CdSe superlattices. The reduced screening of the electric field in the case of strong epitaxial connections between the NCs was recently invoked to explain that the absorptance of a 2D superlattice approaches the absorptance quantum ($\pi\alpha$, where α is the fine structure constant) observed with semiconductor quantum wells [P.T. Prins *et al.*, Nano Lett. **21**, 9426 (2021)]. We conclude that atomically coherent superlattices have a strong light absorption and emission, even in the NC monolayer limit, and are primary candidates for polarization-selective photodetectors and LEDs.

DOI: 10.1103/PhysRevB.107.245413

I. INTRODUCTION

A main strategy in nanomaterial science is to assemble nanoscale building blocks into unique materials to generate physical, chemical, or biological properties which cannot be found in materials synthesized by more conventional routes [1–6]. In self-assembled systems, some properties can be directly retraced to those of the building blocks, while other properties, called collective properties, emerge from the interactions between the building blocks in the assembly. Here we demonstrate that colloidal semiconductor nanocrystals (NCs) [7–12] and their self-assembled lattices form a remarkable platform to study properties resulting from the dielectric (and quantum) coupling between the NC building blocks. It is already known that dipolar coupling between neighbor NCs strongly influences the optical properties in monolayers of disconnected NCs [13,14]. The permeation in NCs can also be enhanced by a matrix with a high dielectric constant. Along this line, we show that, in atomically coherent superlattices obtained by oriented attachment of NCs, the dielectric screening of in-plane electromagnetic fields can be considerably reduced due to the epitaxial connections between neighbor NCs. This results in a strongly enhanced absorptance, approaching that of semiconductor quantum wells.

Here, we present atomistic calculations of the dielectric response in one-dimensional (1D) and two-dimensional (2D) NC superlattices of different geometries. We deduce that the local field in superlattices is strongly enhanced with respect to the cases of single NCs and monolayers of unattached NCs. We also present tight-binding calculations of the optical absorptance of square lattices of PbSe (CdSe) NCs and propose a simple analytic model for the lowest-energy absorption peak. By comparison with measured data [15], we show that lattices of epitaxially connected NCs are characterized by approximately the same oscillator strengths as dispersed NCs but have considerably higher local-field factors. We also evaluate the excitonic effects in the particular case of NC dimers. We conclude that atomically coherent superlattices of NCs are promising materials for cost-effective photodetectors,

*christophe.delerue@iemn.fr

 ©2023 American Physical Society

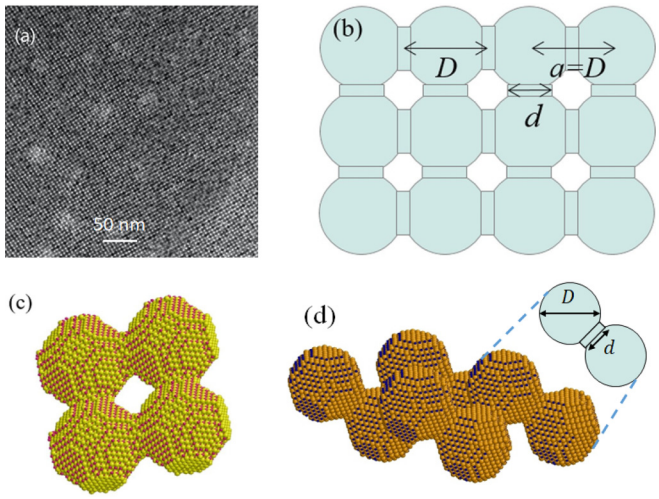

FIG. 1. (a) Typical overview bright-field transmission electron microscopy image on a square superlattice. The average size of the NCs is 5.6 nm, the width of the connections between NCs is typically half this value. (b) Model for square lattices of spherical NCs (diameter D) linked by cylindrical connections (diameter d). The superlattice parameter a is equal to D. (c) Atomistic view of a square superlattice of NCs. (d) Atomistic view of a honeycomb (silicene-type) superlattice made of spherical NCs. The [111] crystallographic axis is perpendicular to the lattice plane. Each NC of the top layer (sub-lattice A) is attached to three NCs of the bottom layer (sub-lattice B) along the [-100], [0-10] and [00-1] directions, the three connections being made with cylinders of diameter d, the angle between NC–NC bonds being 90° [39]

not only for their tunable energy spectrum and their improved transport properties compared to assemblies of disconnected NCs [16] but also for their high absorptance, relatively close to the upper limit corresponding to the perfectly crystalline thin film (nanowire) in 2D (1D) systems, thanks to a reduced screening of the electric component of the external electromagnetic field. The present study of the permeation of the electromagnetic field in low-dimensional semiconductors is inspired by the recent findings [15] that this upper limit for band-edge absorptance in 2D systems such as graphene [17], semiconductor quantum wells [18,19] and atomically coherent superlattices of NCs have a universal character directly related to the absorptance quantum $\pi\alpha$, where α is the fine structure constant.

II. NC SUPERLATTICES

A. Experimental situation

In the present paper, we consider 1D and 2D materials obtained by oriented attachment of NCs to form bigger crystals [20–25]. This approach was particularly successful with the lead chalcogenide family PbX (hereafter, X=S, Se, Te). As illustrated in Fig. 1(a), monolayers of PbX NCs forming 2D square superlattices can be synthesized using presently well-established methodologies [11,23,26–30]. The superlattices, formed by the attachment via (100) facets of NCs with a truncated cubic shape, are characterized by a great homogeneity on a large scale, as shown, for example, in Fig. 1(a). Remarkably, 2D silicene-type honeycomb structures can also be synthesized using the same building blocks [11,29,31]. In that case, the axis perpendicular to the superlattice is along a [111] crystallographic direction but the NCs are still connected via (100) facets, and the adjacent NC–NC bonds form an angle of 90°. The syntheses of multilayers of square lattices [32], 3D superlattices [33], linear and zigzag chains [29], and dimer molecules [34] are also reported. Furthermore, NC superlattices of CdX can be produced from PbX ones using a cation exchange process [11,35]. Direct atomic attachment of wurtzite CdSe NCs to form NC dimers or NC artificial solids was also reported recently [36].

B. Band structure

Owing to the periodic character of NC superlattices in the absence of disorder, band-structure theory can be used to describe their electronic states [37–39]. In the case of PbX compounds, the highest valence band and the lowest conduction band can be well understood using an effective tight-binding model in which each NC is seen as an artificial atom characterized by hole and electron states with S-like envelope wave function [40]. In the lattice, the electronic coupling between neighbor NCs leads to the formation of minibands, called S bands for those derived from NC S states. This simple description also holds for the lowest conduction miniband in CdX or HgX NC superlattices [37–41]. The width of these minibands is directly related to the NC–NC coupling strength [37–39,42]. In the following, we will demonstrate that dielectic screening properties are also strongly influenced by the epitaxial connections between neighbor NCs.

III. METHODOLOGY

A. Atomic model of the superlattices

Even if as-prepared PbX NCs have a truncated cubic shape, structural characterizations reveal a substantial atomic rearrangement during the oriented attachment process that creates necking at NC–NC interfaces and final NC shapes are approximately spherical [21,31]. Like in our previous works on band-structure calculations [38–41], this effect is taken into account by modeling the NCs as spheres connected by cylinders to form the superlattice [Fig. 1(b)]. The diameter D of each NC is equal to 5.5 nm for PbSe, 6.1 nm for CdSe, close to the experimentally reported sizes [11,21,39,43]. The diameter d of the cylinders is taken as a parameter ($0 \leqslant d \leqslant D$), allowing us to tune the coupling between neighbor NCs. The ratio d/D is typically of the order of 0.5 in synthesized superlattices [43]. The atomic structure is defined by considering all the atoms of the crystal (rocksalt or zinc blende) included within the spheres of diameter D and the cylinders of diameter d.

B. Calculation of the dielectric response

Our main goal in this paper is to calculate the dielectric response of single NCs and superlattices of NCs to an external electric field E_0 of angular frequency ω. We characterize this response by the so-called local-field factor $F = \bar{E}/E_0$, where $\bar{E}$ is the average internal field in the semiconductor compound. F is smaller than 1 because the electromagnetic field pushes

polarization charges against the outer planes of each NC, resulting in a depolarization field that partly neutralizes the driving field.

The calculation of the dielectric response cannot be done using a quantum mechanical approach because the investigated systems contain thousands of atoms. Following Ref. [44], we thus use a semiempirical model in which the dielectric response is described by polarizable bonds between the atoms. This methodology was assessed by comparison with more elaborate descriptions [44–46]. For an isolated NC, it gives a local-field factor very close to its classical value,

$$F(\text{isolated NC}) = \frac{3\varepsilon_M}{2\varepsilon_M + \varepsilon'_{\text{in}}}, \tag{1}$$

where $\varepsilon'_{\text{in}} \equiv \text{Re}[\varepsilon_{\text{in}}(\omega)]$ is the real part of the dielectric permittivity of the semiconductor compound at the frequency ω, and ε_M is the dielectric permittivity of the surrounding medium. This atomistic model was also successfully used to describe the polarizability of optically excited InAs NCs [47].

In this approach, we describe a dielectric system as an ensemble of N atoms. We define on each atom i the average (energy) potential V_i which is related to the variations of charge δn_j on all atoms j, i.e., the induced polarization charges. As described in Refs. [44,45], each physical quantity in this atomistic model is thus described by a matrix of size N. The bare potential V_0 induced by the external field E_0, the screened potential V, and the charges δn are all defined by a column matrix of length N. The potentials and charges are linked by the linear relation $\delta n = \chi V$, where χ is the $N \times N$ polarization matrix that describes the noninteracting density response function. The screened potential, from which we derive $\bar{E}$, is also given by $V = V_0 + v\delta n$, where the matrix v represents electron-electron Coulomb interactions, i.e., $v_{n,m} = e^2/|R_n - R_m|$, where R_n is the position of atom n. Combining these equations leads to $V = \varepsilon^{-1}V_0$, where ε is the $N \times N$ dielectric matrix equal to $I - v\chi$, where I is the identity matrix. As described in Ref. [44], the nondiagonal terms of χ are restricted to nearest neighbors, and the bond polarizability is adjusted to give the correct dielectric constant ε'_{in} for the bulk semiconductor.

Since superlattices are usually deposited on a substrate, polarization charges in the semiconductor are accompanied by their image charges in the substrate. We thus add their contribution to the Coulomb matrix v. In the present paper, we consider a quartz substrate (refractive index n_s of 1.46). However, we have found that the substrate has a minor influence on the local-field factor (except for the effect of the reflection of the light, see next section)—image charge effects could be safely neglected. When we consider infinitely extended periodic systems, the matrix equations are rewritten in Fourier space [45]. In that case, N represents the number of atoms per unit cell. The matrix elements of the potentials are calculated using the Ewald summation method [48].

C. Tight-binding calculations of the absorptance

The optical absorptance is the ratio between incident and absorbed light. For a superlattice of NCs deposited on a substrate of refractive index n_s, it can be written as

$$\mathcal{A}(\omega) = F_r^2 F^2 \mathcal{A}_0(\omega), \tag{2}$$

where the first term $F_r^2 = 4/(n_s+1)^2$ accounts for the reflection of the light by the substrate [15,18]. F is here the local-field factor defined with respect to the external field composed of the incident and reflected fields. $\mathcal{A}_0(\omega)$ is the internal absorptance given in the single particle (SP) approximation by [46]

$$\mathcal{A}_0(\omega) = \frac{\pi\hbar e^2}{2mc\varepsilon_0 S} \sum_{\mathbf{k}} \sum_{i,j} f_{i,j}(\mathbf{k}) \delta(\hbar\omega - E_i(\mathbf{k}) + E_j(\mathbf{k})), \tag{3}$$

where $\mathbf{k}$ is the crystal momentum and i (j) runs over conduction (valence) states $|i,\mathbf{k}\rangle$ ($|j,\mathbf{k}\rangle$) of energy $E_i(\mathbf{k})$ ($E_j(\mathbf{k})$), S is the surface of the 2D sample on which we apply periodic boundary conditions, e is the unit charge (electron charge $= -e$), $\hbar$ is the reduced Planck's constant, m is the electron mass, c is the light velocity and ε_0 is the vacuum permittivity. In addition, $f_{i,j}(\mathbf{k})$ is the oscillator strength of the optical transition given by

$$f_{i,j}(\mathbf{k}) = \frac{2m}{\hbar^2}(E_i(\mathbf{k}) - E_j(\mathbf{k}))|\langle j,\mathbf{k}|x|i,\mathbf{k}\rangle|^2 \tag{4}$$

for the optical electric field polarized along x.

The electronic states $|i,\mathbf{k}\rangle$ ($|j,\mathbf{k}\rangle$) are calculated in tight binding using a $sp^3d^5s^*$ basis of atomic orbitals for each spin. We used the model of Ref. [49] (derived from Ref. [37]) for CdSe and Ref. [50] for PbSe. We checked that very similar results are obtained with the tight-binding parameters of Ref. [51] for PbSe. The dipolar matrix elements in Eq. (4) are calculated as described in Refs. [46,52]. In the following, we will also show calculations in which the absorptance spectrum is convoluted by a Gaussian function to account for size dispersion and disorder present in the experimentally synthesized superlattices.

D. Two-level model of the absorptance for the lowest optical transition

In addition to the tight-binding calculations, it is also interesting to consider a simple two-level model for the lowest optical absorption peak of NC superlattices. We assume that the total oscillator strength $\bar{f}$, summed over all transitions contributing to this peak at the energy $\hbar\omega_0$, is the same as in single NCs. $\bar{f}$ was deduced from optical cross sections measured on PbSe [53] and CdSe [54] NCs in solution. For the NC sizes considered in the present paper, $\bar{f}$ is of the order of 16 for both PbSe and CdSe.

From Eq. (3), the internal absorptance line shape is written as

$$\mathcal{A}_0(\omega) = \frac{\pi\hbar e^2}{2mc\varepsilon_0 S_0}\bar{f}\frac{1}{\eta\sqrt{2\pi}}\exp\left[-\frac{(\hbar\omega - \hbar\omega_0)^2}{2\eta^2}\right], \tag{5}$$

where S_0 is the surface occupied by a single NC in the lattice. In this equation, we have replaced the delta function by a Gaussian characterized by the broadening energy η. Combined with Eq. (2), the previous equation leads to

$$\mathcal{A}(\hbar\omega) = \frac{1.75\,F^2}{(n_s+1)^2}\frac{\bar{f}}{S_0\eta}\exp\left[-\frac{(\hbar\omega - \hbar\omega_0)^2}{2\eta^2}\right], \tag{6}$$

where S_0 is given in nm^2, $\hbar\omega_0$ and η in eV.

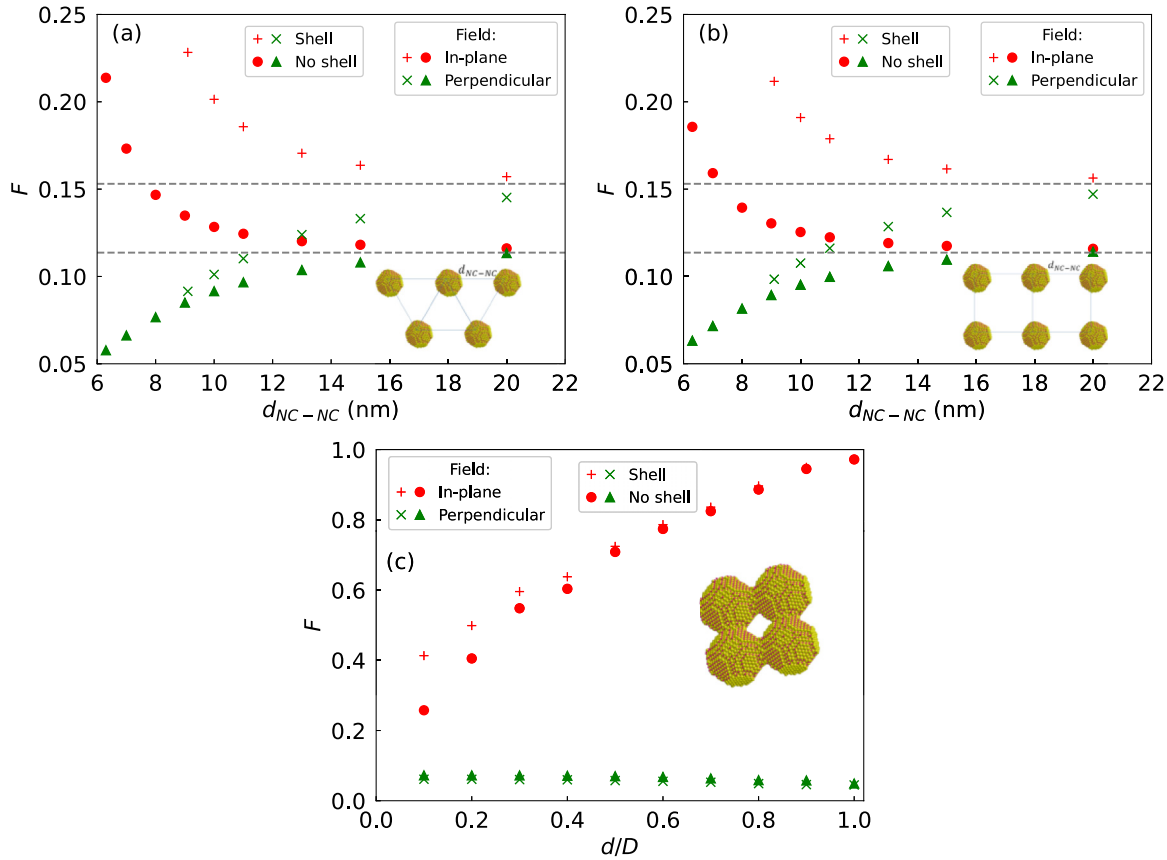

FIG. 2. (a) Evolution of the local-field factor F with the distance $d_{\mathrm{NC-NC}}$ between centers of neighbor NCs in a monolayer of PbSe NCs characterized by an hexagonal lattice. The results are obtained for in-plane (red) or perpendicular (green) fields for uncapped NCs (circles or triangles) or NCs capped with 1.4-nm-thick shell of dielectric permittivity of 2 (+ or ×). The horizontal dashed lines represent the limits at infinite distance. (b) Same for a square lattice. (c) F in a square lattice of epitaxially connected NCs versus the normalized width d/D of the connections between neighbor NCs for perpendicular (green) or in-plane (red) field. + or ×: F for a superlattice embedded in 6.4-nm-thick layer of dielectric permittivity of 2.

E. Excitonic effects

To estimate the excitonic effects on the optical absorption spectra, we performed calculations using a configuration interaction (CI) approach. The results of these calculations in the case of dimers of NCs are discussed in Sec. VII. The starting point is the calculation of SP states by the tight-binding method as described above. These SP states are used to construct a basis of Slater determinants. The excitonic states are obtained as linear combinations of the form

$$\left|\Psi^i_{\mathrm{exc}}\right\rangle = \sum_{vc} a^i_{cv} |\psi_{vc}\rangle \tag{7}$$

where $|\psi_{vc}\rangle$ is the Slater determinant that describes the excitation of a single electron from the valence state v to the conduction state c from a reference state where all valence (conduction) states are full (empty). The matrix of the excitonic Hamiltonian is written in this basis taking into account the terms resulting from the Coulomb interactions (self-energy, Coulomb and exchange terms). The details of this CI method have been published in Refs. [55–57].

In the case of the dimers of PbSe NCs (Sec. VII), we consider a basis of 144 valence states and 144 conduction states corresponding to the set of S, P, and D states of each NC taking into account the eightfold degeneracy of the valleys in the conduction and valence bands of PbSe [51]. We consider 36 conduction states and 400 valence states in the case of CdSe NC dimers, with the disymmetry in the number of states reflecting the disymmetry in the effective masses in light conduction and heavy valence bands.

IV. DIELECTRIC SCREENING IN SUPERLATTICES OF PbSe NCs

In this section, we discuss the specific case of PbSe but the conclusions are valid for other semiconductor compounds. We consider the dielectric screening at frequencies close to the lowest interband transitions ($\hbar\omega \approx 0.7$ eV). In this frequency range, it was shown that the dielectric constant in PbSe NCs is close to its bulk value, we therefore use $\varepsilon'_{\mathrm{in}} = 23$ [58].

A. Monolayers of disconnected PbSe NCs

Before looking at NC superlattices, it is interesting to consider monolayers of NCs in which the NCs are disconnected but are assembled on a periodic lattice. By comparison, this will allow us to reveal the effects of epitaxial connections in superlattices synthesized by oriented attachment. We present in Fig. 2(a) results of our calculations for hexagonal lattices

of PbSe NCs. Such monolayers can be prepared by interfacial assembly in the presence of excess oleate capping, in order to prevent oriented attachment [59].

Figure 2(a) shows the evolution of the local-field factor F for an in-plane field when we vary the distance between the NCs, i.e., the hexagonal lattice parameter. At large distance, F is close to F (isolated NC), the expected value for a single NC. Our calculations also demonstrate that F is increased when each NC is surrounded by a dielectric shell which simulates the response of capping ligands [14]. In any case, the internal electric field increases when the distance between NCs decreases due to dipolar coupling between nearest-neighbor NCs [14]. For the close-packed monolayers considered in Fig. 2(a), the enhancement factor compared to the single-NC case can be of the order of 2, which corresponds to a factor of 4 for the absorption ($\propto F^2$). We show in Appendix A that the results of Fig. 2(a) can be quantitatively explained by the analytical theory of Ref. [14] in which each NC is described as a point dipole. Physically, within each NC, a dipole is formed under the action of the external electric field which, in isolated NCs, is strongly decreased by the depolarization field. In the 2D lattices, the depolarization field is reduced by the presence of the dipoles located in the neighboring NCs, and this effect is amplified when the NCs get closer.

Very similar results are obtained for square lattices of disconnected NCs [Fig. 2(b)]. This type of array appears as an intermediate phase during transformation of hexagonal lattices into square superlattices of epitaxially connected NCs by oriented attachment of the NCs [27,60,61].

B. Square lattices of epitaxially connected PbSe NCs

The case of square lattices of epitaxially connected NCs is presented in Fig. 2(c). When the connections between neighbor NCs are very narrow (e.g., $d/D = 0.1$), the local-field factor for a field in the lattice plane is in the range of 0.2–0.3, close to the value found for close-packed square monolayers of disconnected NCs [Fig. 2(b)]. In other words, narrow connections have a small effect on dielectric properties. The presence of a thin embedding layer (dielectric permittivity of 2) mimicking capping ligands tends to reduce the screening but F remains around 0.4. Increasing the width of the connections leads to a significant enhancement of the local-field factor, which reaches a value close to 1 for $d/D = 1$. In that case, we recover a situation close to a pristine PbSe quantum well. In a dielectric film, an in-plane field is totally unscreened ($F = 1$) since the polarization charges are repelled at infinity (in reality, at a distance of the order of the light wavelength, large compared to d). On the contrary, for a field perpendicular to the film, screening is very efficient, $F = 1/\varepsilon'_{\text{in}}$ (0.04 for PbSe). This is also found in square superlattices of NCs for which we find values of F well below 0.1 for a perpendicular field. In this case, F varies from $3/(2+\varepsilon'_{\text{in}})$ for $d/D \to 0$ to $\approx 1/\varepsilon'_{\text{in}}$ for $d/D \to 1$.

From the three panels of Fig. 2, we see that the local-field factor varies from 0.11 (0.15 with a shell) for PbSe NCs dispersed on the substrate to 0.71 (0.72 with a shell) for PbSe NCs in a square superlattice with $d/D = 0.5$. The term F^2 contributing to the optical cross section (absorption) thus varies by a factor of 42 (23 with a shell) between the two situations, which represents a broad range.

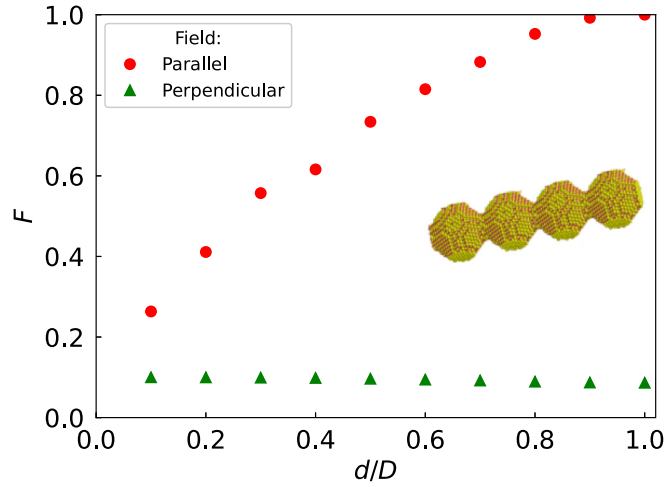

FIG. 3. Local-field factor F in a linear chain of PbSe NCs versus the normalized width d/D of the connections between neighbor NCs for a field along the chain (red dots) or perpendicular to it (green triangles).

C. Chains of epitaxially connected PbSe NCs

The same effects are predicted in 1D systems. Figure 3 shows that the local-field factor strongly increases with d/D for a field applied along a chain of epitaxially connected PbSe NCs. F is exactly equal to 1 for $d/D = 1$, when the chain becomes a cylindrical wire and the totality of the polarization charges is pushed at the edges of the cylinder (here infinity). On the contrary, F remains small for a field perpendicular to the chain. If the chain is irradiated with linearly polarized light, we thus predict a huge dependence of the absorption on the angle θ between the electric field and the chain axis. Indeed, the oscillator strength contains a term $|\langle \bar{\mathbf{E}} \cdot \mathbf{p} \rangle|^2$, where $\bar{\mathbf{E}}$ is the mean internal electric field, $\mathbf{p}$ the momentum operator, and $\langle\rangle$ represents the matrix element between the initial and final states of the transition. This term thus behaves as $(F_\parallel \langle p_\parallel \rangle \cos(\theta) + F_\perp \langle p_\perp \rangle \sin(\theta))^2$, where $F_\parallel$ ($F_\perp$) is the local-field factor for parallel (perpendicular) polarization, $\langle p_\parallel \rangle$ and $\langle p_\perp \rangle$ are the transition matrix elements of the momentum operator along the two directions. In experimental situations where $d/D < 0.8$, the matrix elements $\langle p_\parallel \rangle$ and $\langle p_\perp \rangle$ are very close (see below), so the oscillator strength varies approximately as $\cos^2(\theta)$ since $F_\parallel \gg F_\perp$.

D. Bilayers of square superlattices of epitaxially connected PbSe NCs

The case of square superlattices made of a bilayer of PbSe NCs is also interesting (Fig. 4). We have considered the case where NCs are epitaxially connected not only in the lattice plane but also between the two superposed layers, since this is realized experimentally [32,33,40]. We find that local-field factor remains close to its value for single square lattices [Fig. 2(c)]. We conclude that the amount of absorbed light per layer is the same in bilayer superlattices than in single layer ones, in agreement with experimental observations [15].

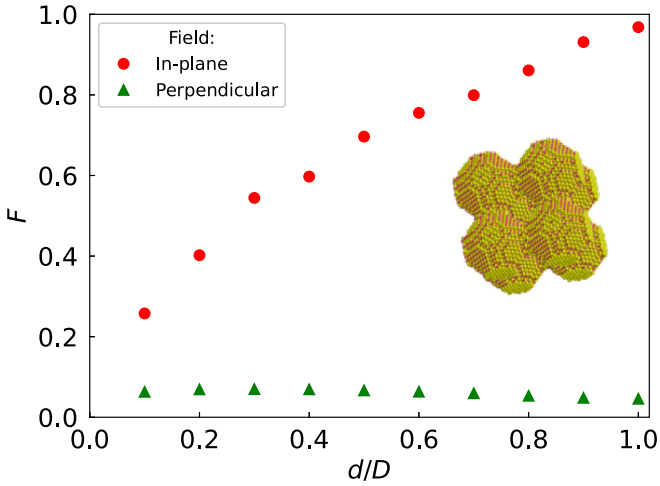

FIG. 4. Local-field factor F in a bilayer of square superlattices of PbSe NCs versus the normalized width d/D of the connections between neighbor NCs for a field along the bilayer (red dots) or perpendicular to it (green triangles).

E. Honeycomb lattices of epitaxially connected PbSe NCs

In silicene-type honeycomb lattices of epitaxially connected PbSe NCs, the two NCs of the unit cell are not in the same plane. The connections between neighbor NCs are not parallel to the (111) lattice plane. As a consequence, we expect a smaller effect of the epitaxial connections on the dielectric screening than in square superlattices. This is confirmed in Fig. 5 showing that, for an in-plane field, the local-field factor F still increases with d/D but with a smaller slope than in Fig. 2(b). The maximum value attained for $d/D = 1$ is 0.79, due to the presence of polarization charges which remain in each unit cell due to the buckled atomic structure of the lattice, characterized by NC–NC bonds along [100] directions and which result in a nonzero depolarization field. The values of F for a perpendicular field (along [111]) remain small, like in the case of square lattices.

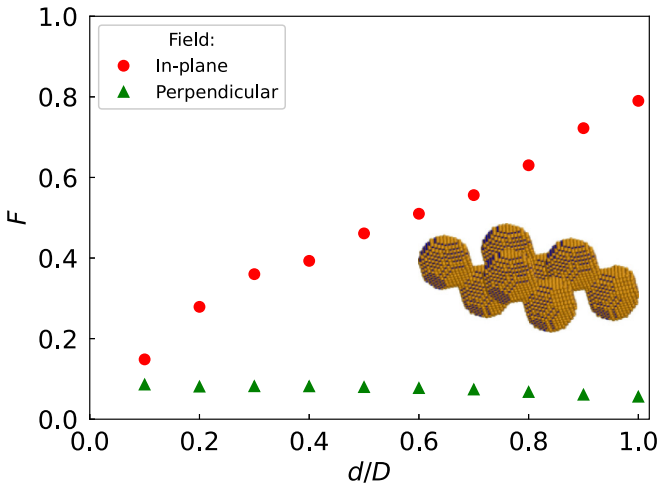

FIG. 5. Local-field factor F in a honeycomb (silicene-type) superlattice of PbSe NCs versus the normalized width d/D of the connections between neighbor NCs for a field in plane (red dots) or perpendicular to it (green triangles).

V. CALCULATIONS OF THE OPTICAL ABSORPTANCE IN 2D SUPERLATTICES

Absorptance spectra of superlattices were measured in Ref. [15]. Those for square lattices of epitaxially connected PbSe and CdSe NCs are reproduced in Figs. 6(a) and 6(b), respectively. Those for a bilayer of square lattices and a honeycomb lattice of epitaxially connected PbSe are depicted in Figs. 6(c) and 6(d), respectively. They are representative for a series of measurements recorded independently by different research groups (see Supporting Information S3 of Ref. [15]). Figure 6 also shows the results of tight-binding calculations for comparison (Table I). Relatively good agreement is obtained when we take into account some broadening which can be attributed to disorder and size dispersion. It should be noted that we chose the d/D ratio to have the lowest energy absorption peak in good agreement with the experiment. A slightly larger value of d/D (e.g., 0.6 instead of 0.5) would allow us to have better agreement at higher energy by globally increasing the absorption intensity, at the expense of the concordance at low energy. In any case, this ratio d/D remains close to what was obtained by structural analysis [42,43].

Remarkably, as partially shown in our previous study [15], Fig. 6 also demonstrates that the lowest peak in the measured absorptance spectra can be very-well described by the two-level model of Sec. III D, for both PbSe and CdSe, for square (monolayer or bilayer) or honeycomb lattices. This means that total oscillator strength in this peak is approximately the same for NC superlattices as for NCs in colloidal solution, which can be understood by the origin of the superlattice minibands in terms of NC states (Secs. II B and VII). Therefore, the increase in optical absorption in superlattices compared to isolated NCs comes mainly from the significant increase in the local field factor.

The discrepancies between tight-binding calculations and experiments could be due, in principle, to inaccuracies of tight-binding parametrizations, the lack of excitonic corrections in the calculations, or a limited description of the complex dielectric environment of NC superlattices. However, the calculations presented in Sec. VII and in Appendix B show that excitonic effects are probably too small to explain the observed differences. Since the theory-experiment agreement is good with the two-level model, we can also infer that the local field effects are rather well-described. We conclude that the errors more likely come from the tight-binding description. The agreement with the experimental results is nevertheless already very satisfactory considering the approximations inherent to this semiempirical method and the differences between the different measurements (Supporting Information S3 of Ref. [15]).

The scales on the right of the panels in Fig. 6 represent the absorptance $\mathcal{A}$ divided by $F_r^2 F^2 \pi\alpha$. $\mathcal{A}/(F_r^2 F^2)$ is in fact the internal absorptance $\mathcal{A}_0$ [Eq. (2)], i.e., the response to the internal field. As discussed in Ref. [15], we see that $\mathcal{A}_0$ at the lowest peak is close to $2\pi\alpha$ for the square and honeycomb superlattices of PbSe NCs, $\pi\alpha$ for the square lattice of CdSe NCs, corresponding to the limits obtained for the quantum

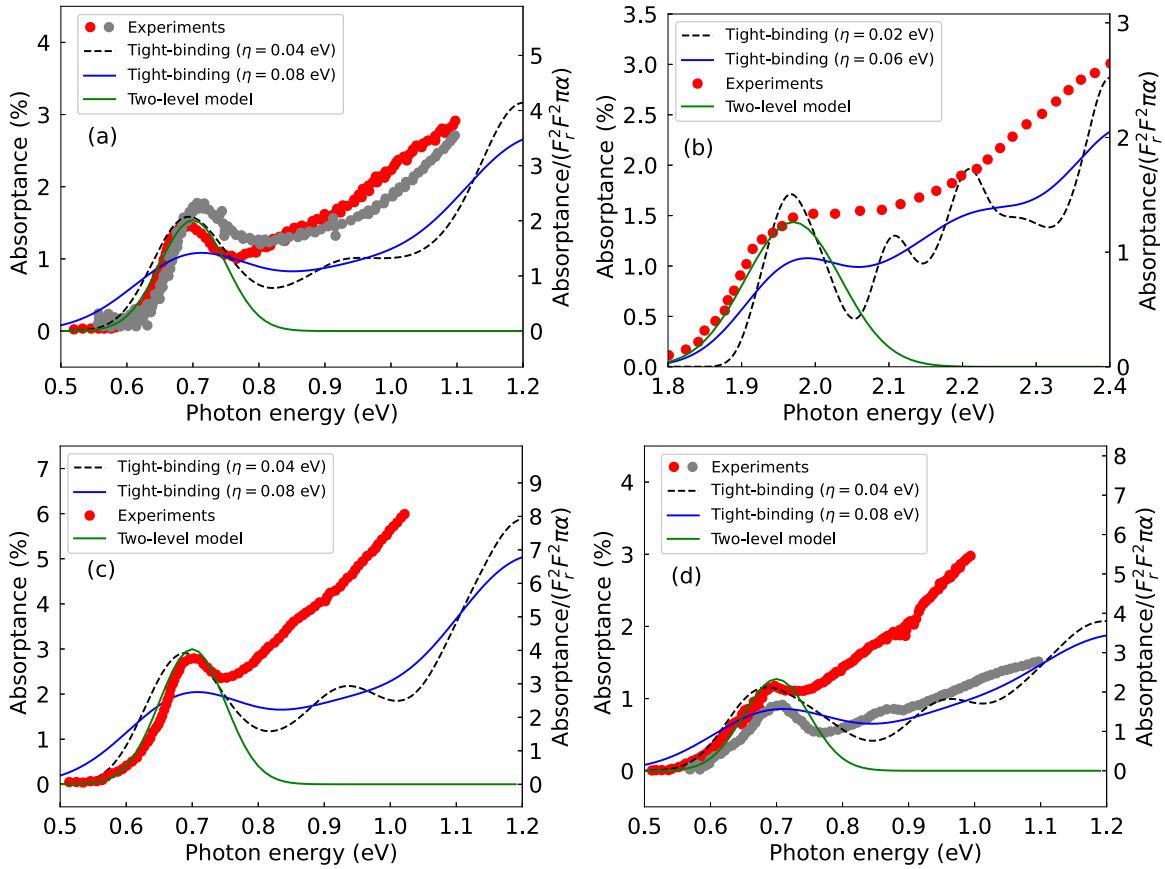

FIG. 6. Absorptance of square superlattices of PbSe NCs (a), square superlattices of CdSe NCs (b), bilayers of square superlattices of PbSe NCs (c), and honeycomb (silicene-type) superlattices of PbSe NCs (d). Red and grey dots: Representative sets of experimental results [15]. Blue solid lines and black dashed lines: Tight-binding calculations for superlattices deposited on a quartz substrate and embedded in a layer of dielectric permittivity of 2. Green solid lines: Calculations using the two-level model. The parameters used for the calculations are given in Table I. In all panels, the right-hand scale represents the absorptance $\mathcal{A}$ divided by $F_r^2 F^2 \pi\alpha$, i.e., the internal absorptance $\mathcal{A}_0$ [Eq. (2)] divided by the absorption quantum $\pi\alpha$. By definition, the two-level model (green solid line) describes only the $S_h - S_e$ transitions forming the lowest energy absorption peak.

wells of PbSe and CdSe, respectively [19]. A value close to $4\pi\alpha$ is found for the bilayer of PbSe NCs [Fig. 6(b)]. The physical origin of this remarkable behavior is discussed in Refs. [15,19].

VI. ABSORPTION ENHANCEMENT IN LATTICES OF EPITAXIALLY CONNECTED NCs

We conclude from the previous section that NCs in solution or in superlattices are characterized by similar oscillator strengths for the lowest optical transition. However, NCs in atomically coherent superlattices absorb a considerably larger amount of light (about a factor of 10) than in solution because the local-field factor is larger, i.e., the electric field component of the light is less screened. This is demonstrated in Fig. 7, where we plot the absorption enhancement factor for a square lattice of epitaxially connected NCs ($d/D = 0.5$) compared to the same NCs dispersed at the surface of the substrate, i.e., in the absence of NC–NC coupling. This enhancement factor is defined as the ratio between the optical cross sections obtained in the two situations. Assuming similar oscillator strengths, transition energies, and peak broadening, this factor simplifies into the ratio of the squared local-field factors.

TABLE I. Calculated values of F and parameters used for the calculation of the theoretical data of Fig. 6.

				Tight-binding calculations			Two-level model		
Figure	Lattice	Compound	F	D (nm)	d/D	η (eV)	$\hbar\omega_0$ (eV)	$\bar{f}$	η (eV)
Fig. 6(a)	Square	PbSe	0.71	5.5	0.5	0.04 or 0.08	0.70	16	0.05
Fig. 6(b)	Square	CdSe	0.87	6.1	0.6	0.02 or 0.06	1.97	16	0.065
Fig. 6(c)	Square bilayer	PbSe	0.70	5.5	0.5	0.04 or 0.08	0.70	16 × 2	0.05
Fig. 6(d)	Honeycomb	PbSe	0.60	5.5	0.6	0.04 or 0.08	0.70	16	0.05

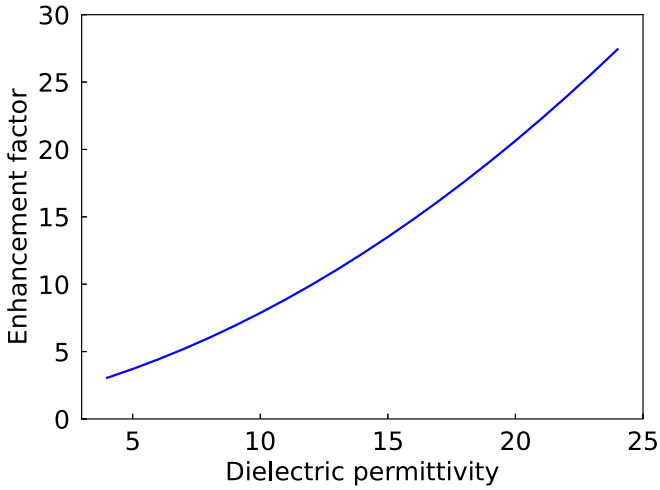

FIG. 7. Enhancement factor of the optical absorption in a square NC superlattice ($D = 6$ nm, $d/D = 0.5$) with respect to the same NCs present as individual NCs on the substrate surface, as function of the dielectric permittivity of the NC semiconductor compound. To simulate the effect of the ligands, each individual NC is surrounded by a 1.4-nm-thick shell and the square lattice is embedded in a 8.8-nm-thick dielectric film (dielectric permittivity = 2).

The enhancement factor is the largest when the NCs are composed of a semiconductor compound characterized by a high dielectric permittivity (Fig. 7). Then it can reach very high values, above 20. In any case, we conclude as in Ref. [15] that lattices of epitaxially connected NCs are very appealing materials for the realization of efficient photodetectors, in particular, since the enhanced absorption can be combined with a higher carrier mobility.

VII. EFFECT OF EXCITONIC CORRECTIONS: THE CASE OF A DIMER OF PbSe NCs

One can wonder if the epitaxial connections between NCs have a great influence on the electron-electron and electron-hole interactions, thus on the excitonic effects, since they have some on the dielectric screening. One can also wonder if excitonic effects contribute to the discrepancy between experimental results and tight-binding calculations in Fig. 6. Dealing with this question goes far beyond the objectives of the present paper, especially since the calculation of excitonic effects in NC superlattices is complex due to their large size and infinite extension in two dimensions. Nevertheless, we considered a simpler case consisting of a dimer of PbSe NCs because it allows us to study the effect of a variable diameter connection while being numerically treatable by the CI method described in Sec. III E. The results of this section are presented taking into account a low broadening ($\eta = 5$ meV) which reveals the main structures of absorption peaks but does not allow us to distinguish fine structures of excitonic transitions as in Ref. [62]. We have shown previously that much higher values are needed to represent the experimental situation characterized by a substantive inhomogeneous broadening.

Figure 8(c) shows that, even if it is less than in NC chains (Fig. 3) and especially in square lattices of NCs [Fig. 2(c)], the effect on the dielectric screening of the epitaxial connection between neighboring NCs is still important in the dimer case. This explains on the one hand that the optical absorption is much more important for a light polarized parallel to the dimer axis [Fig. 8(a)] than perpendicularly [Fig. 8(b)], on the other hand that the absorption for a parallel polarization increases in intensity when d/D increases [Fig. 8(a)]. This behavior is the same with or without excitonic effects.

The influence of excitonic effects on the optical spectra is relatively minor, resulting mainly in a shift towards low energies [Figs. 8(a) and 8(b)]. The behavior of the spectra is quite similar with and without excitonic effects, although differences in shape are clearly visible. The low energy absorption peaks ($0.6 - 0.8$ eV) correspond to transitions from the eight S_h states originating from the L valleys of the valence band to the eight S_e states coming from the conduction band valleys, and this for each NC. These states (valence or conduction) are not degenerate because of the intervalley couplings whose intensity depends not only on the size of the NCs but also on their symmetry and surface structuring [50,51,62–64]. The situation becomes even more complicated in the dimer case due to the fact that each S_e (or S_h) state of a NC couples to its equivalent in the neighboring NC to form a symmetric (bonding) and an antisymmetric (antibonding) state. These states are then coupled together by the Coulomb and exchange terms of the excitonic Hamiltonian.

The obtained spectra resulting from $(2 \times 8) \times (2 \times 8)$ transitions depend quite significantly on the shape and the surface of the NCs. Nevertheless, for $d/D \to 1$, the dominant effect becomes the coupling between neighboring NCs and the low-energy spectrum is limited to two main peaks corresponding on the one hand to transitions between symmetric states (valence-conduction) and on the other hand to transitions between antisymmetric states. For intermediate values of d/D, the effect of the epitaxial connection between NCs is a broadening and a shift towards low energies of the $S_h - S_e$ peak, as observed experimentally and modeled in a simplified approach [34]. Figure 8(d) presents an experimental spectrum for a NC sample containing ≈23% dimers formed by the fusion of monomers of estimated diameter 5.8 nm. We superimpose on these results our calculations for $D = 5.5$ nm and several values of d/D for comparison. Although the variability in size and shape is unknown, it is clear that the experimental results can be reasonably interpreted by our calculations for relatively wide connections (>0.5).

The weak influence of excitonic effects in dimers of PbSe NCs is explained by the fact that these systems remain in strong quantum confinement regime for which excitonic corrections mainly result in a shift of the spectra and in a mixing limited to the states of the same multiplet coming from different valleys but characterized by the same envelope function. Mixing between S and P multiplets, for example, remains weak for d/D values lower than 0.8.

In the case of coherent NC superlattices of PbSe NCs, the states of each multiplet (S, P) form energy bands well separated from each other [37,38,65,66]. The intervalley couplings induce the lifting of degeneracy between subbands but without preventing this separation. We therefore expect identical conclusions about the excitonic effects in these 2D systems.

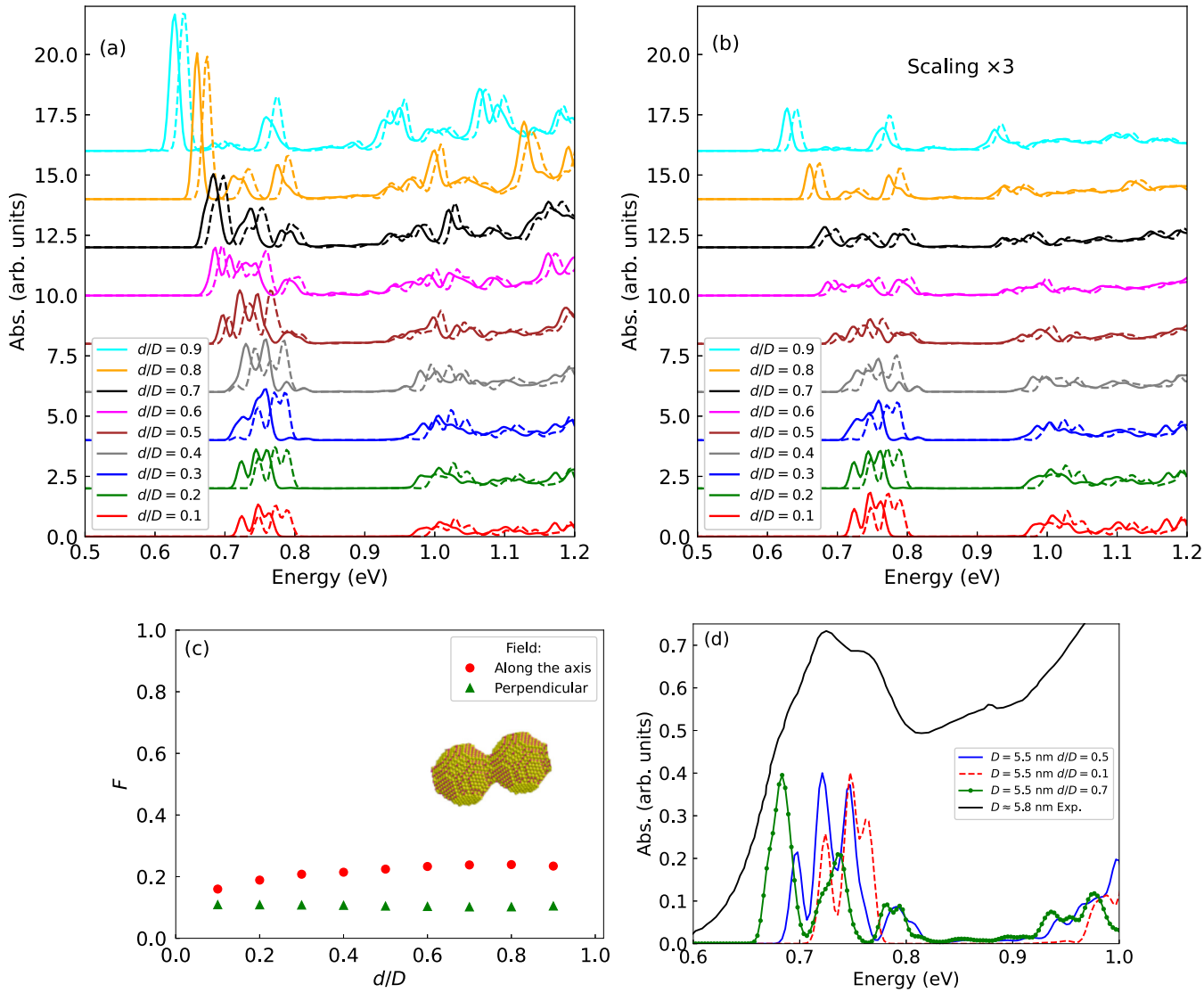

FIG. 8. (a) Optical absorption spectrum of dimers of PbSe NCs (of slightly different diameters, $D = 5.5$ nm and $D' = 0.97D$), for different values of the normalized width d/D of the connections between the NCs for light polarized along the axis of the dimer (solid lines: excitonic calculations; dashed lines: single-particle calculations). (b) Same for a polarization perpendicular to the dimer axis. All curves of (a) and (b) are plotted using the same vertical scale but data of (b) are multiplied by a factor 3. (c) Local-field factor F for an electric field along the axis of the dimer (red dots) or perpendicular to it (green triangles). (d) Experimental spectrum for a sample of PbSe NCs (diameter ≈5.8 nm) containing ≈23% dimers [34] (black solid line) compared to results of calculations for $d/D = 0.1$ (red dashed line), $d/D = 0.5$ (blue solid line), and $d/D = 0.7$ (green dotted solid line). In all calculations, the broadening η is set at 5 meV to reveal fine structures.

The strong quantum confinement effects that result from low electron and hole masses and the strongly screened Coulomb interactions explain the weak excitonic effects in PbSe NC arrays. Appendix B shows that these effects are more important in the case of CdSe, a material characterized by a lower dielectric constant and much heavier hole masses.

VIII. CONCLUSION

In this paper, we have shown that the epitaxial connections in superlattices of semiconductor NCs have a profound effect on the dielectric properties. The local-field factor F, defined as the ratio between internal and external fields, strongly increases with the diameter d of the connections between NCs for in-plane fields. While F is of the order of 0.2–0.3 in 2D close-packed arrays of disconnected ($d \to 0$) PbSe and CdSe NCs at their optical threshold, F increases to about 0.7–0.8 in square superlattices presenting a strong epitaxial connection between neighbor NCs ($d/D \approx 0.5$), which is supported by the good agreement between calculated absorptance spectra and experimental data. Owing to their high optical absorptance ($\propto F^2$) and electrical conductivity, atomically coherent superlattices of NCs are promising materials for the realization of low-cost photodetectors. This conclusion is supported by our recent work showing that the optical absorptance of these superlattices approaches the semiconductor quantum well limit which, when corrected for local field factors, is directly related to the universal quantity $\pi\alpha$, where α is the fine-structure constant [15].

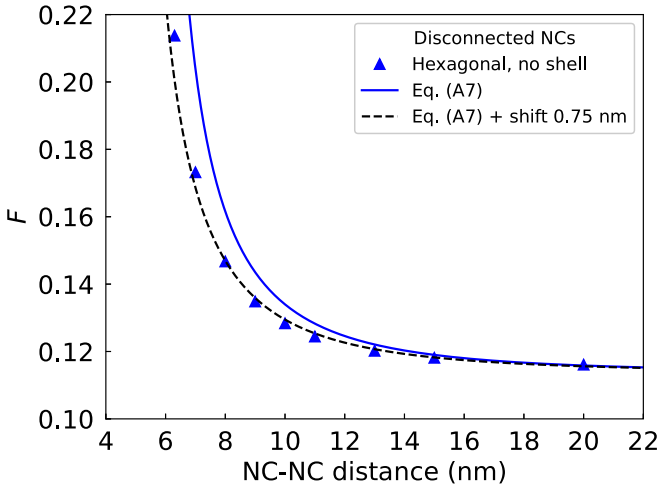

FIG. 9. Evolution of the local-field factor F with the distance between centers of neighbor NCs in a monolayer of PbSe NCs characterized by a hexagonal lattice (uncapped NCs). Blue triangles: Present numerical calculations [same as in Fig. 2(a)]. Blue solid line: Analytic formula [Eq. (A7) with $\varepsilon_M = 1$] derived from the dipolar model of Ref. [14]. Black dashed line: Same curve shifted 0.75 nm to smaller NC–NC distance.

APPENDIX A: CROSS SECTION OF NCs IN A MONOLAYER OF DISCONNECTED NCs

In the case of a monolayer of disconnected NCs, the local-field factor can be calculated analytically by approximating each NCs by a polarizable dipole. We assume that the monolayer is embedded in a medium of dielectric permittivity ε_M. Following Ref. [14], the dipole moment of a NC under the external field E_0 of angular frequency ω is given by

$$\mathcal{P}(\omega) = \varepsilon_M \alpha(\omega) E_L, \tag{A1}$$

where E_L is the in-plane component of the field which includes, in addition to E_0, the dipolar contribution of neighboring NCs. $\alpha(\omega)$ is the net polarizability

$$\alpha(\omega) = 4\pi\varepsilon_0 R^3 \frac{\varepsilon_{\text{in}}(\omega) - \varepsilon_M}{\varepsilon_{\text{in}}(\omega) + 2\varepsilon_M}, \tag{A2}$$

where R is the NC radius and $\varepsilon_{\text{in}}(\omega)$ is the complex permittivity of the semiconductor compound. Since E_L is the same on each NC (for lattices with one NC per unit cell), E_L is a solution of the following equation:

$$E_L = E_0 + \alpha(\omega) S E_L. \tag{A3}$$

S is a (dipolar) lattice sum over all contributions from the neighboring NCs [14],

$$S = \frac{1}{4\pi\varepsilon_0} \sum_i \frac{3\cos(\theta_i)^2 - 1}{d_i^3}, \tag{A4}$$

where d_i is the distance of the neighbor i on the lattice and θ_i is the angle of the vector $\mathbf{d}_i$ to the neighbor with respect to the direction of the external field. E_L is thus given by $E_0/(1 - \alpha(\omega)S)$. The cross section of a NC in the monolayer is given by [14]

$$\sigma_F(\omega) = \frac{\omega\varepsilon_M}{c\varepsilon_0 n_M} \text{Im}\left[\frac{\alpha(\omega)}{1 - S\alpha(\omega)}\right], \tag{A5}$$

where $n_M = \sqrt{\varepsilon_M}$ is the refractive index of the host medium. If S_0 is the area of the surface occupied by one NC, the absorptance is given by

$$\mathcal{A}(\omega) = \sigma_F(\omega)/S_0. \tag{A6}$$

The term $1/(1 - \alpha(\omega)S)$ in Eq. (A5) represents the enhancement factor of the electric field in a monolayer of NCs with respect to the isolated NC situation for which the local-field factor was given by F(isolated NC) [Eq. (1)]. We thus

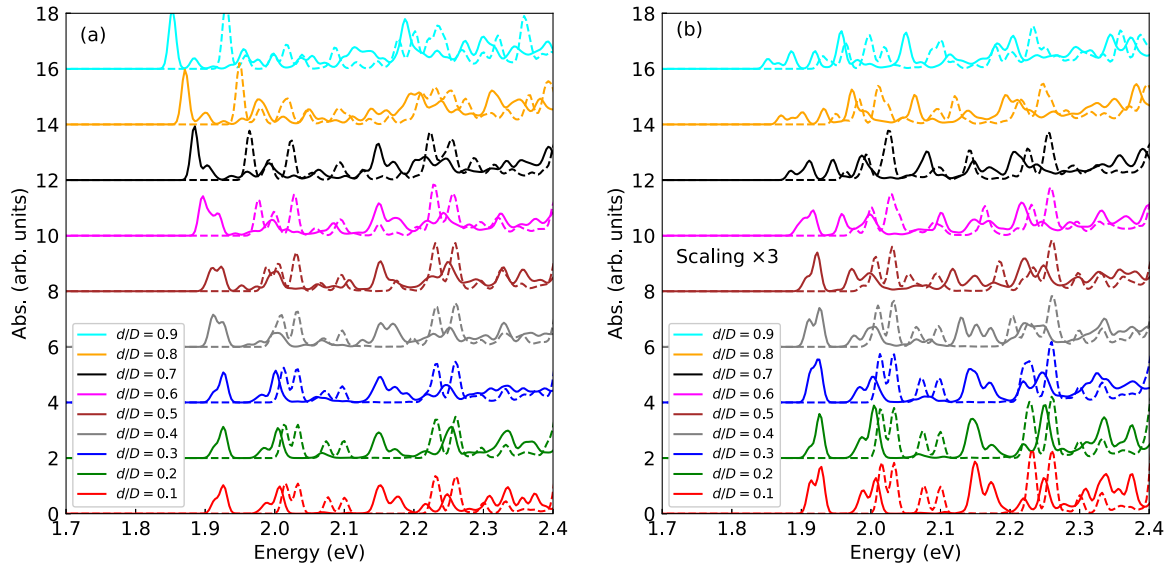

FIG. 10. (a) Optical absorption spectrum of dimers of CdSe NCs (of slightly different diameters, $D = 6.1$ nm and $D' = 0.97D$), for different values of d/D, for a light polarized along the axis of the dimer (solid lines: excitonic calculations; dashed lines: single-particle calculations). (b) Same for a polarization perpendicular to the dimer axis. All curves of (a) and (b) are plotted using the same vertical scale but data of (b) are multiplied by a factor of 3. In all calculations, the broadening η is set at 5 meV to reveal fine structures.

deduce the local-field factor in a monolayer embedded in a uniform environment of permittivity ε_M:

$$F = \left(\frac{1}{1 - \mathrm{Re}[\alpha(\omega)]S}\right)\frac{3\varepsilon_M}{2\varepsilon_M + \varepsilon'_{\mathrm{in}}}. \tag{A7}$$

This equation, and therefore the local-field model discussed in the present paper, is valid when the imaginary part of $1 - S\alpha(\omega)$ is small compared to the real part. This is typically the case for band-edge optical transitions. This is no longer valid otherwise, in particular, at the resonance, i.e., when $1 - \mathrm{Re}[\alpha(\omega)]S \to 0$, a case which was investigated in Ref. [14] (see also Ref. [67] for 3D lattices of NCs).

Figure 9 shows that Eq. (A7) explains the variations of the local-field factor in a monolayer of disconnected NCs with the NC–NC distance. An even better agreement between analytic and numerical calculations is obtained when we apply a small rigid shift (0.75 nm) to the analytic curve. This shift can be interpreted by modifications of dielectric properties that appear close to the surface of the NCs [46,68].

APPENDIX B: EFFECT OF EXCITONIC CORRECTIONS: THE CASE OF A DIMER OF CdSe NCs

Figure 10 shows that excitonic effects are more prominent in CdSe NC dimers than in PbSe ones. The shift of the spectra to low energies is larger, and the differences in the shape of the absorption peaks between SP and excitonic models are more pronounced. This is due to the low dielectric constant and heavy effective mass of holes in CdSe compared to PbSe. Since the distance between hole states in the valence band is smaller, the mixing between states induced by Coulomb interactions is larger. Nevertheless, the excitonic effects on the shape and intensity of the absorption peaks remain quite modest overall, in particular, if we consider a larger broadening compatible with the experimental spectra.

[1] S. C. Glotzer, Some assembly required, Science **306**, 419 (2004).

[2] S. C. Glotzer and M. J. Solomon, Anisotropy of building blocks and their assembly into complex structures, Nat. Mater. **6**, 557 (2007).

[3] M. Rycenga, C. M. Cobley, J. Zeng, W. Li, C. H. Moran, Q. Zhang, D. Qin, and Y. Xia, Controlling the synthesis and assembly of silver nanostructures for plasmonic applications, Chem. Rev. **111**, 3669 (2011).

[4] S. Guo and S. Sun, FePt nanoparticles assembled on graphene as enhanced catalyst for oxygen reduction reaction, J. Am. Chem. Soc. **134**, 2492 (2012).

[5] M. A. Boles, M. Engel, and D. V. Talapin, Self-assembly of colloidal nanocrystals: From intricate structures to functional materials, Chem. Rev. **116**, 11220 (2016).

[6] F. Li, J. Lu, X. Kong, T. Hyeon, and D. Ling, Dynamic nanoparticle assemblies for biomedical applications, Adv. Mater. **29**, 1605897 (2017).

[7] N. Zaitseva, Z. R. Dai, F. R. Leon, and D. Krol, Optical properties of CdSe superlattices, J. Am. Chem. Soc. **127**, 10221 (2005).

[8] E. V. Shevchenko, D. V. Talapin, N. A. Kotov, S. O'Brien, and C. B. Murray, Structural diversity in binary nanoparticle superlattices, Nature (London) **439**, 55 (2006).

[9] J. J. Urban, D. V. Talapin, E. V. Shevchenko, and C. B. Murray, Self-assembly of PbTe quantum dots into nanocrystal superlattices and glassy films., J. Am. Chem. Soc. **128**, 3248 (2006).

[10] C. Schliehe, B. H. Juarez, M. Pelletier, S. Jander, D. Greshnykh, M. Nagel, A. Meyer, S. Foerster, A. Kornowski, C. Klinke, and H. Weller, Ultrathin PbS sheets by two-dimensional oriented attachment, Science **329**, 550 (2010).

[11] W. H. Evers, B. Goris, S. Bals, M. Casavola, J. de Graaf, R. van Roij, M. Dijkstra, and D. Vanmaekelbergh, Low-dimensional semiconductor superlattices formed by geometric control over nanocrystal attachment, Nano Lett. **13**, 2317 (2013).

[12] T. Hanrath, Colloidal nanocrystal quantum dot assemblies as artificial solids, J. Vac. Sci. Technol., A **30**, 030802 (2012).

[13] C. Delerue and G. Allan, Effective dielectric constant of nanostructured Si layers, Appl. Phys. Lett. **88**, 173117 (2006).

[14] P. Geiregat, Y. Justo, S. Abe, S. Flamee, and Z. Hens, Giant and broad-band absorption enhancement in colloidal quantum dot monolayers through dipolar coupling, ACS Nano **7**, 987 (2013).

[15] P. T. Prins, M. Alimoradi Jazi, N. A. Killilea, W. H. Evers, P. Geiregat, W. Heiss, A. J. Houtepen, C. Delerue, Z. Hens, and D. Vanmaekelbergh, The fine-structure constant as a ruler for the band-edge light absorption strength of bulk and quantum-confined semiconductors, Nano Lett. **21**, 9426 (2021).

[16] W. H. Evers, J. M. Schins, M. Aerts, A. Kulkarni, P. Capiod, M. Berthe, B. Grandidier, C. Delerue, H. S. J. van der Zant, C. van Overbeek, J. L. Peters, D. Vanmaekelbergh, and L. D. A. Siebbeles, High charge mobility in two-dimensional percolative networks of PbSe quantum dots connected by atomic bonds, Nat. Commun. **6**, 8195 (2015).

[17] R. R. Nair, P. Blake, A. N. Grigorenko, K. S. Novoselov, T. J. Booth, T. Stauber, N. M. R. Peres, and A. K. Geim, Fine structure constant defines visual transparency of graphene, Science **320**, 1308 (2008).

[18] H. Fang, H. A. Bechtel, E. Plis, M. C. Martin, S. Krishna, E. Yablonovitch, and A. Javey, Quantum of optical absorption in two-dimensional semiconductors, Proc. Natl. Acad. Sci. USA **110**, 11688 (2013).

[19] M. Lannoo, P. T. Prins, Z. Hens, D. Vanmaekelbergh, and C. Delerue, Universality of optical absorptance quantization in two-dimensional group-IV, III-V, II-VI, and IV-VI semiconductors, Phys. Rev. B **105**, 035421 (2022).

[20] D. Li, M. H. Nielsen, J. R. I. Lee, C. Frandsen, J. F. Banfield, and J. J. De Yoreo, Direction-specific interactions control crystal growth by oriented attachment., Science **336**, 1014 (2012).

[21] C. S. S. Sandeep, J. M. Azpiroz, W. H. Evers, S. C. Boehme, I. Moreels, S. Kinge, L. D. A. Siebbeles, I. Infante, and A. J. Houtepen, Epitaxially connected PbSe quantum-dot films: Controlled neck formation and optoelectronic properties, ACS Nano **8**, 11499 (2014).

[22] P. Schapotschnikow, M. A. van Huis, H. W. Zandbergen, D. Vanmaekelbergh, and T. J. H. Vlugt, Morphological transformations and fusion of PbSe nanocrystals studied using atomistic simulations, Nano Lett. **10**, 3966 (2010).

[23] W. J. Baumgardner, K. Whitham, and T. Hanrath, Confined-but-connected quantum solids via controlled ligand displacement, Nano Lett. **13**, 3225 (2013).

[24] D. M. Balazs, D. N. Dirin, H.-H. Fang, L. Protesescu, G. H. ten Brink, B. J. Kooi, M. V. Kovalenko, and M. A. Loi, Counterion-mediated ligand exchange for PbS colloidal quantum dot superlattices, ACS Nano **9**, 11951 (2015).

[25] W. Walravens, J. De Roo, E. Drijvers, S. ten Brinck, E. Solano, J. Dendooven, C. Detavernier, I. Infante, and Z. Hens, Chemically triggered formation of two-dimensional epitaxial quantum dot superlattices, ACS Nano **10**, 6861 (2016).

[26] M. A. Sliem, A. Chemseddine, U. Bloeck, and R. A. Fischer, PbSe nanocrystal shape development: oriented attachment at mild conditions and microwave assisted growth of nanocubes, CrystEngComm **13**, 483 (2011).

[27] J. J. Geuchies, C. van Overbeek, W. H. Evers, B. Goris, A. de Backer, A. P. Gantapara, F. T. Rabouw, J. Hilhorst, J. L. Peters, O. Konovalov, A. V. Petukhov, M. Dijkstra, L. D. A. Siebbeles, S. van Aert, S. Bals, and D. Vanmaekelbergh, In situ study of the formation mechanism of two-dimensional superlattices from PbSe nanocrystals, Nat. Mater. **15**, 1248 (2016).

[28] E. K. Wujcik, S. R. Aceto, R. Narayanan, and A. Bose, Lead selenide nanostructures self-assembled across multiple length scales and dimensions, J. Nanomater. **2016**, 1 (2016).

[29] C. van Overbeek, J. L. Peters, S. A. P. van Rossum, M. Smits, M. A. van Huis, and D. Vanmaekelbergh, Interfacial self-assembly and oriented attachment in the family of PbX (X = S, Se, Te) nanocrystals, J. Phys. Chem. C **122**, 12464 (2018).

[30] K. Whitham, D.-M. Smilgies, and T. Hanrath, Entropic, enthalpic, and kinetic aspects of interfacial nanocrystal superlattice assembly and attachment, Chem. Mater. **30**, 54 (2018).

[31] M. P. Boneschanscher, W. H. Evers, J. J. Geuchies, T. Altantzis, B. Goris, F. T. Rabouw, S. A. P. van Rossum, H. S. J. van der Zant, L. D. A. Siebbeles, G. Van Tendeloo, I. Swart, J. Hilhorst, A. V. Petukhov, S. Bals, and D. Vanmaekelbergh, Long-range orientation and atomic attachment of nanocrystals in 2D honeycomb superlattices, Science **344**, 1377 (2014).

[32] B. H. Savitzky, R. Hovden, K. Whitham, J. Yang, F. Wise, T. Hanrath, and L. F. Kourkoutis, Propagation of structural disorder in epitaxially connected quantum dot solids from atomic to micron scale, Nano Lett. **16**, 5714 (2016).

[33] A. Abelson, C. Qian, T. Salk, Z. Luan, K. Fu, J.-G. Zheng, J. L. Wardini, and M. Law, Collective topo-epitaxy in the self-assembly of a 3D quantum dot superlattice, Nat. Mater. **19**, 49 (2020).

[34] B. K. Hughes, J. L. Blackburn, D. Kroupa, A. Shabaev, S. C. Erwin, A. L. Efros, A. J. Nozik, J. M. Luther, and M. C. Beard, Synthesis and spectroscopy of PbSe fused quantum-dot dimers, J. Am. Chem. Soc. **136**, 4670 (2014).

[35] D. H. Son, S. M. Hughes, Y. Yin, and A. Paul Alivisatos, Cation exchange reactions in ionic nanocrystals., Science **306**, 1009 (2004).

[36] J. C. Ondry, J. P. Philbin, M. Lostica, E. Rabani, and A. P. Alivisatos, Resilient pathways to atomic attachment of quantum dot dimers and artificial solids from faceted CdSe quantum dot building blocks, ACS Nano **13**, 12322 (2019).

[37] E. Kalesaki, W. H. Evers, G. Allan, D. Vanmaekelbergh, and C. Delerue, Electronic structure of atomically coherent square semiconductor superlattices with dimensionality below two, Phys. Rev. B **88**, 115431 (2013).

[38] C. Delerue, From semiconductor nanocrystals to artificial solids with dimensionality below two, Phys. Chem. Chem. Phys. **16**, 25734 (2014).

[39] C. Delerue and D. Vanmaekelbergh, Electronic band structure of zinc blende CdSe and rock salt PbSe semiconductors with silicene-type honeycomb geometry, 2D Mater. **2**, 034008 (2015).

[40] A. Tadjine and C. Delerue, Colloidal nanocrystals as LEGO ® bricks for building electronic band structure models, Phys. Chem. Chem. Phys. **20**, 8177 (2018).

[41] W. Beugeling, E. Kalesaki, C. Delerue, Y.-M. Niquet, D. Vanmaekelbergh, and C. M. Smith, Topological states in multi-orbital HgTe honeycomb lattices, Nat. Commun. **6**, 6316 (2015).

[42] W. Walravens, E. Solano, F. Geenen, J. Dendooven, O. Gorobtsov, A. Tadjine, N. Mahmoud, P. P. Ding, J. P. C. Ruff, A. Singer, G. Roelkens, C. Delerue, C. Detavernier, and Z. Hens, Setting carriers free: Healing faulty interfaces promotes delocalization and transport in nanocrystal solids, ACS Nano **13**, 12774 (2019).

[43] K. Whitham, J. Yang, B. H. Savitzky, L. F. Kourkoutis, F. Wise, and T. Hanrath, Charge transport and localization in atomically coherent quantum dot solids, Nat. Mater. **15**, 557 (2016).

[44] G. Allan and C. Delerue, Energy transfer between semiconductor nanocrystals: Validity of Förster's theory, Phys. Rev. B **75**, 195311 (2007).

[45] C. Delerue, M. Lannoo, and G. Allan, Calculations of the electron-energy-loss spectra of silicon nanostructures and porous silicon, Phys. Rev. B **56**, 15306 (1997).

[46] C. Delerue and M. Lannoo, *Nanostructures: Theory and Modeling* (Springer, Berlin, 2004).

[47] J. J. H. Pijpers, M. T. W. Milder, C. Delerue, and M. Bonn, (Multi)exciton dynamics and exciton polarizability in colloidal InAs quantum dots, J. Phys. Chem. C **114**, 6318 (2010).

[48] P. P. Ewald, Die berechnung optischer und elektrostatischer gitterpotentiale, Ann. Phys. **369**, 253 (1921).

[49] M. Dufour, E. Izquierdo, C. Livache, B. Martinez, M. G. Silly, T. Pons, E. Lhuillier, C. Delerue, and S. Ithurria, Doping as a strategy to tune color of 2D colloidal nanoplatelets, ACS Appl. Mater. Interfaces **11**, 10128 (2019).

[50] A. N. Poddubny, M. O. Nestoklon, and S. V. Goupalov, Anomalous suppression of valley splittings in lead salt nanocrystals without inversion center, Phys. Rev. B **86**, 035324 (2012).

[51] G. Allan and C. Delerue, Confinement effects in PbSe quantum wells and nanocrystals, Phys. Rev. B **70**, 245321 (2004).

[52] M. Graf and P. Vogl, Electromagnetic fields and dielectric response in empirical tight-binding theory, Phys. Rev. B **51**, 4940 (1995).

[53] I. Moreels, K. Lambert, D. De Muynck, F. Vanhaecke, D. Poelman, J. C. Martins, G. Allan, and Z. Hens, Composition and size-dependent extinction coefficient of colloidal PbSe quantum dots, Chem. Mater. **19**, 6101 (2007).

[54] R. Karel Čapek, I. Moreels, K. Lambert, D. De Muynck, Q. Zhao, A. Van Tomme, F. Vanhaecke, and Z. Hens, Optical properties of zincblende cadmium selenide quantum dots, J. Phys. Chem. C **114**, 6371 (2010).

[55] E. Martin, C. Delerue, G. Allan, and M. Lannoo, Theory of excitonic exchange splitting and optical stokes shift in silicon nanocrystallites: Application to porous silicon, Phys. Rev. B **50**, 18258 (1994).

[56] E. Groeneveld, C. Delerue, G. Allan, Y.-M. Niquet, and C. de Mello Donegá, Size dependence of the exciton transitions in colloidal CdTe quantum dots, J. Phys. Chem. C **116**, 23160 (2012).

[57] G. Allan and C. Delerue, Tight-binding calculations of the optical properties of HgTe nanocrystals, Phys. Rev. B **86**, 165437 (2012).

[58] I. Moreels, G. Allan, B. De Geyter, L. Wirtz, C. Delerue, and Z. Hens, Dielectric function of colloidal lead chalcogenide quantum dots obtained by a Kramers-Krönig analysis of the absorbance spectrum, Phys. Rev. B **81**, 235319 (2010).

[59] G. Soligno and D. Vanmaekelbergh, Phase diagrams of honeycomb and square nanocrystal superlattices from the nanocrystal's surface chemistry at the dispersion-air interface, J. Chem. Phys. **151**, 234702 (2019).

[60] J. C. daSilva, M. A. Smeaton, T. A. Dunbar, Y. Xu, D. M. Balazs, L. F. Kourkoutis, and T. Hanrath, Mechanistic insights into superlattice transformation at a single nanocrystal level using nanobeam electron diffraction, Nano Lett. **20**, 5267 (2020).

[61] J. C. Ondry, J. P. Philbin, M. Lostica, E. Rabani, and A. P. Alivisatos, Colloidal synthesis path to 2D crystalline quantum dot superlattices, ACS Nano **15**, 2251 (2021).

[62] I. D. Avdeev, M. O. Nestoklon, and S. V. Goupalov, Exciton fine structure in lead chalcogenide quantum dots: Valley mixing and crucial role of intervalley electron-hole exchange, Nano Lett. **20**, 8897 (2020).

[63] K. Overgaag, D. Vanmaekelbergh, P. Liljeroth, G. Mahieu, B. Grandidier, C. Delerue, and G. Allan, Electron-phonon coupling and intervalley splitting determine the linewidth of single-electron transport through pbse nanocrystals, J. Chem. Phys. **131**, 224510 (2009).

[64] S. V. Goupalov, E. L. Ivchenko, and M. O. Nestoklon, Optical transitions, exciton radiative decay, and valley coherence in lead chalcogenide quantum dots, Phys. Rev. B **106**, 125301 (2022).

[65] E. Kalesaki, C. Delerue, C. Morais Smith, W. Beugeling, G. Allan, and D. Vanmaekelbergh, Dirac Cones, Topological Edge States, and Nontrivial Flat Bands in Two-Dimensional Semiconductors with a Honeycomb Nanogeometry, Phys. Rev. X **4**, 011010 (2014).

[66] M. Alimoradi Jazi, V. A. E. C. Janssen, W. H. Evers, A. Tadjine, C. Delerue, L. D. A. Siebbeles, H. S. J. van der Zant, A. J. Houtepen, and D. Vanmaekelbergh, Transport properties of a two-dimensional PbSe square superstructure in an electrolyte-gated transistor, Nano Lett. **17**, 5238 (2017).

[67] C. Delerue, G. Allan, and Y. M. Niquet, Collective excitations in charged nanocrystals and in close-packed arrays of charged nanocrystals, Phys. Rev. B **72**, 195316 (2005).

[68] C. Delerue, M. Lannoo, and G. Allan, Concept of dielectric constant for nanosized systems, Phys. Rev. B **68**, 115411 (2003).